On the Electronic and Optical Properties of Metal-Organic Frameworks: Case Study of MIL-125 and MIL-125-NH_2

Gloria Capano,[†,#] Francesco Ambrosio,[‡,¶,§,#] Stavroula Kampouri,[∥] Kyriakos C. Stylianou,[∥] Alfredo Pasquarello,[⊥] and Berend Smit[*,∥]

†*Laboratory of molecular simulation (LSMO) - Ecole Polytechnique Fédérale de Lausanne(EPFL)*

‡*Chaire de Simulation à l'Echelle Atomique(CSEA), Ecole Polytechnique Fédérale de Lausanne(EPFL)*

¶*Computational Laboratory for Hybrid/Organic Photovoltaics (CLHYO), Istituto CNR di Scienze e Tecnologie Molecolari (ISTM-CNR), Via Elce di Sotto 8, 06123 Perugia, Italy*

§*CompuNet, Istituto Italiano di Tecnologia, Via Morego 30, 16163 Genova, Italy*

∥*Laboratory of molecular simulation (LSMO) - Ecole polytechnique Fédérale de Lausanne(EPFL)*

⊥*Chaire de Simulation à l'Echelle Atomique(CSEA), Ecole polytechnique Fédérale de Lausanne(EPFL)*

#*Contributed equally to this work*

E-mail: alfredo.pasquarello@epfl.ch,berend.smit@epfl.ch

Abstract

The photoactive MIL-125 and MIL-125-NH_2 Metal-Organic Frameworks (MOFs), despite a very similar crystalline structure, exhibit different optically behaviour. Luminescence in MIL-125 decays in about 1 ns while for its amino counterpart the lifetime of the charge-carriers is at least one order of magnitude larger.[1] The origin of this difference is the key element for understanding the photocatalytic behaviour of MIL-125-NH_2 when associated with active nanoparticles, behaviour that is completely absent in MIL-125.[2] By performing advanced ab-initio electronic structure calculations, we find that charge-carriers interact differently in the two MOFs with subsequent effects on the luminescence lifetimes and their catalytic performances. To confirm the predictions of our model we synthesized a novel material in the MIL-125 family, MIL-125-NH_2-[10%]$(OH)_2$, and confirm that our theory correctly predicts a faster decay compared to MIL-125-NH_2.

Introduction

Photo-induced hydrogen water splitting is a promising alternative to standard electrolysis techniques.[3–5] The photocatalytic production of hydrogen proceeds following three steps: i) sunlight absorption and generation of charge carriers (electrons, e-, and holes, h+), ii) migration of the charge carriers to the catalytic active sites, iii) reduction reaction of water with subsequent H_2 production and parallel oxidation reaction in order to neutralize the remaining negative charge of the photogenerated electron.[6–10] In this context, large efforts have been devoted to the search for the ideal photocatalyst material. Among them, Metal-Organic-Frameworks (MOFs), have attracted the attention of a growing scientific community because of their possible application in an expanding range of fields.[11–13]

MOFs are crystalline materials, formed by organic molecules, the linkers, connected by inorganic metal-oxide nodes. Their modular structure allows to study of singular components and their interactions can improve their chemical-physical performances. In the field of

photoinduced catalysis many studies have been carried in this direction.[14–18]

In this context, a photocative MOF absorbs photons, and then photo-generated electrons are injected into a catalytic nanoparticle. The water reduction reaction occurs on the surface of the nanoparticles, while the hole is captured by a hole scavenger dissolved into the solution. This composite metal-organic frameworks/metallic nanoparticles, MOFs/NPs system, detains the actual record of molar hydrogen production under solar illumination.[2] In this system, the MOF, MIL-125-NH_2 (MIL = Materials of Institute Lavoisier)[19] act as the antenna and the catalyst is phosphorus oxide nanoparticles.

MIL-125 is formed by cyclic octamers of TiO_2 octahedra linked by 1,4-benzenedicarboxylate (bdc) (Fig. 1). The substitution of the linker with the monoaminated bdc-NH_2 forms the MOF MIL-125-NH_2,[13,20] used in the composite system. Interestingly, this chemical modification appears to be quintessential for the efficiency of the photocatalytic process.[2,8,12,21,22] In fact, the de-aminated MIL-125, while possessing a very similar crystalline structure, is not able to produce any hydrogen. This might be correlated to a different electronic and optical behaviour. Indeed, recent experiments have pointed out that the amino group is able to stabilize the hole leading to an efficient charge separation of the photoexcited electron and hole, a stabilization that is missing for the de-aminated MIL-125.[23] In addition, the lifetime of the charge-carriers is at least one order of magnitude larger in MIL-125-NH_2 than in MIL-125 (about 1 ns).[1,24] These fascinating results show that an apparently small chemical modification of the linker might have a large impact on the electronic and optical properties of a material, making then an essential difference in its technical performances.

From a practical point of view, these results can have significant importance allowing us to enhance specific properties, in this case charge separation, by simply operating a chemical substitution. To fully exploit the potential of such a chemical modification, it is desirable to have a detailed molecular understanding of this behavior. Such an understanding, would hopefully avoid an elaborate *trial and error* to identify an optimal linker.

A large number of high-throughput studies have been deployed to perform computational

screenings aimed at fine-tuning the opto-electronic properties of MOFs.[25–29] These studies have focussed on the effect of linker functionalization on the structural and electronic properties of MOFS have received a profound attention,.[30–35] In particular, theoretical studies have shown that the band gap of MIL-125 can be tuned by adding different functional groups to the bdc.[28] The main drawback of most studies is the use of computational protocols featuring an approximated treatment of the electronic structure, which may only give qualitative results. Furthermore, thermal effects on the electronic structure are usually neglected, an approximation that might provide another possible source of errors.[36,37]

Overall, while previous studies provide important qualitative information, the use approximated methods prevent from achieving a comprehensive explanation regarding the effects of chemical modifications on the optoelectronic properties of this class of MOFs. In addition, at present we do not even have a qualitative theoretical understanding why the lifetimes of the electron/hole pair that is formed after photo excitation in these materials are so different. In this context, the approximated methods commonly employed would provide an incorrect description of charge localization and its energetics, due to the self-interaction error affecting semi-local density functionals[38,39] but also hybrid functionals, if the fraction of Fock-exchange is not correctly determined (e.g. Ref.[40]). Therefore, the current lack of in-depth studies prevents the opto-electronic properties of MOFs and their correlation with the chemical modifications from being completely understood.

In this work, we develop a theoretical framework to qualitatively predict the effects of the functionalization of the ligand on the electronic and optical properties of MOFs. As particular example we aim to obtain a detailed molecular understanding why the electronic and optical properties of MIL-125 and MIL-125-NH_2 are so different. The electronic and optical properties of MIL-based MOFs are still far from being completely understood and their correlation with the chemical modifications has not been rationalized yet. Theoretical studies have shown that the band gap of MIL-125 can be tuned by adding different functional groups to the bdc.[41] However, while these studies provide important qualitative information,

the conventional methods use approximated methods which are not capable of explaining these drastic effects of chemical modifications on the optoelectronic properties of these class of MOFs. In addition, at present we do not even have a theoretical understanding why the lifetimes of the electron-hole pair that is formed after photo excitation in these materials are so different.

We calculate the electronic structure of MIL-125 and MIL-125-NH_2 using advanced hybrid functional calculations.[42] To ensure that calculations of the frontier orbitals, or in band-structure terms, the top of the valence band (VB) and the bottom of the conduction band (CB), respectively, are not biased by the self-interaction error, we derive the amount of Fock exchange to be included in the PBE0 functional from physical considerations based on the Koopman's condition.[43] The challenges in correctly describing the fundamental energy gap of MOFs, without such a bias-free methodology, have been discussed by several authors[41,44–46] In fact, very often, the only experimental information that is provided is the optical gap that has a very different nature from the fundamental one, making even harder to compare energy levels and experiments. Our method provides us with a direct determination of Fock exchange that allows us to compute the optical gap in striking agreement with the experimental one reported previously.[41]

The fact that we are able to obtain such a detailed molecular explanation of the optical and photoexcited state properties of this class of complex materials, illustrates the remarkable progress that has been made in this field. In addition, we apply our theory to predict the lifetime of an electron hole of a novel material in the MIL-125 family and subsequent experiments nicely confirm our predictions.

In this work, we employ an advanced theoretical framework, which enables us to unravel the underlying physical processes that are responsible for the different opto-electronic properties of MIL-125 and MIL-125-NH_2. We first calculate the fundamental and optical band gap of MIL-125 and MIL-125-NH_2 in striking agreement with the experiment. To achieve this goal, we employ density functional theory (DFT) and linear-response-time-dependent-

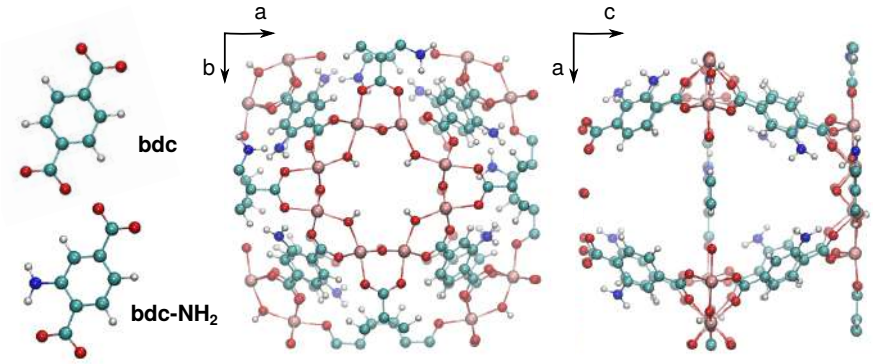

Figure 1: Left: The linkers composing MIL-125 (bdc) and MIL-125-NH_2 (bdc-NH_2). Center and Right: Crystal structure of MIL-125-MOFs. Color code: C cyan, O red, N blue, H white, and Ti pink.

DFT (LR-TDDFT) calculations based on a hybrid functional in which the fraction of Fock exchange is determined from physical considerations, in order to eliminate the noxious self-interaction error which affect standard DFT. Then, by analyzing the nature of charge carriers in both materials, we observe that, upon excitation, the hole and the electron localize in spatially distinct regions of MIL-125-NH_2, while they are largely overlapping in MIL-125. This explains the lower recombination rate experimentally measured for MIL-125-NH_2. In addition, we estimate from LR-TDDFT calculations the ratio of the recombination times for the two materials, obtaining an order of magnitude of difference, a value consistent with the measured lifetimes. These quantitive results are of particular importance as the method that we developed allows us to predict the effects of changes in the linker on the life-time of the electron and the hole.

Methodology and Energy Gap Calculation

We calculate the electronic structure of MIL-125 and MIL-125-NH_2 using advanced PBE0-based hybrid functional calculations. To ensure that calculations of the frontier orbitals, or in band-structure terms, the top of the valence band (VB) and the bottom of the conduction band (CB), respectively, are not biased by the self-interaction error, we derive the amount of Fock exchange to be included in the PBE0 functional from physical considerations based

on the Koopman's condition.[43] Following Refs. 42,47,48, we first inject an extra electron or an extra hole to MIL-125. Then, we relax the structures employing the PBE0 functional with a large fraction of Fock exchange (see for more details SI), observing charge localization in both cases. Next, we keep the achieved structures fixed, and determine the fraction α for which the single particle energy level associated with the extra electron or extra hole does not vary upon occupation, as required by exact density functional theory. We obtain $\alpha = 0.36$ for the electron polaron and α=0.32 for the hole polaron (see SI). Therefore, in the subsequent calculations the average value $\alpha = 0.34$ is used. More details can be found in the SI.

First, we analyse the electronic density of states at 0 K. The calculated projected density of states in Fig. 2 shows that the lowest energy region of the CB of both MIL-125 and MIL-125-NH_2 has a large contribution from the metal cluster formed by Ti(3d) and O(2p) atoms. The π orbitals of the bdc units form the highest energy peak of the VB of MIL-125. The presence of the amino group $-NH_2$ introduces an additional band inside the gap, about 1.3 eV above the linker(π) band, as previously observed.[41] In terms of crystalline orbitals, the HOCO is composed of the molecular π orbitals and the lowest unoccupied crystalline orbital (LUCO) principally of the Ti(3d) and O(2p) orbitals (Fig. 2, top panel).

The calculated fundamental band gap is 5.40 eV and 4.25 eV for MIL-125 and MIL-125-NH_2, respectively. These values are drastically different from those recently reported.[41] However, the available experiments are performed at room temperature and correspond to optical absorption measurements, while the calculations were done at 0 K and they reported fundamental band gaps.

To make a comparison with the experiments it is important to take into account the effect of temperature on the band gap. Following the previous work by Wiktor et al.,[37,49] we define the fundamental band gap at room temperature as:

$$E_{gap}(T) = E_g^0 + \Delta^T + \Delta^{NQE}, \tag{1}$$

where E_g^0 is the fundamental energy gap at 0 K, Δ^T and Δ^{NQE} are the band gap renormalizations induced by the thermal effect and the quantum motion of the nuclei. These terms are calculated by linear extrapolation of the density of states achieved from classical (Δ^T) and path-integral molecular dynamics ($\Delta^T + \Delta^{NQE}$) simulations at room temperature (see the SI for more details). In Fig. 3, we illustrate the renormalization of the density of states of MIL-125 for both methods. The calculated renormalization is sizeable, amounting to 0.37 eV for the pure thermal effect, and 0.75 eV for the thermal and quantum nuclei effects (Table 1). Since the two MOFs are very similar, we employ the calculated corrections of MIL-125 also for MIL-125-NH_2. The resulting fundamental gap is 4.65 eV and 3.50 eV for MIL-125 and MIL-125-NH_2, which is still almost 1 eV larger than the measured values.

This difference is ascribed to the fact that experimental absorption spectra measure the optical band gap, while from the density of states we obtain the fundamental one. The optical band gap is defined as the minimum energy needed to excite an electron from the top of the VB to the bottom of the CB. The optical band gap is smaller than the fundamental band gap, due to the electrostatic interaction between the photogenerated charges (electron and hole). The measured optical band gap is ca. 3.6 eV (345 nm) and 2.6 eV (475 nm)[41] for MIL-125 and MIL-125-NH_2, respectively. We calculate the optical band gap using LR-TDDFT as implemented in the CP2K code.[50] We find that the 0 K optical band gap is 4.44 eV and 3.36 eV for MIL-125 and MIL-125-NH_2, respectively. As expected, the 0 K optical band gap is about 1 eV smaller than the 0 K fundamental band gap (Tab. 1) revealing a large excitonic effect, which is consistent with the low density of these materials and with their low dielectric constants (see calculations in the SI). By including the previously computed band gap renormalization, we finally obtain an optical band gap at room temperature of 3.69 eV and 2.61 eV for the MIL-125 and its amino counterpart, in remarkable agreement with the measured optical band gaps (Table 1).

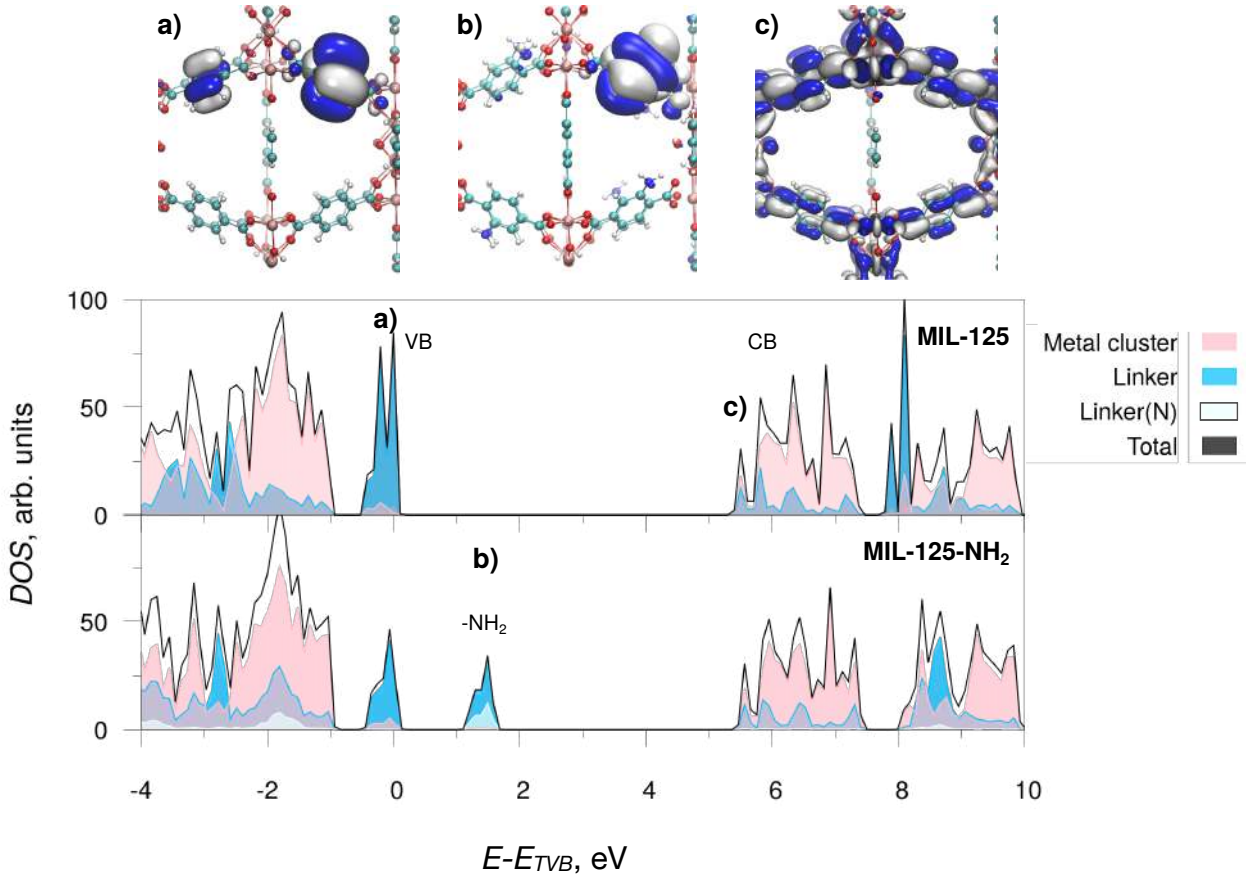

Figure 2: Top panel: Selection of crystalline orbitals: a) MIL-125 HOCO, b) MIL-125-NH_2 HOCO, c) MIL-125- LUCO. Bottom panel: Total density of states and projected density of states of MIL-125 and MIL-125-NH_2. The TVB energy refers to the energy of the top of the valence band of MIL-125; the density of states of MIL-125-NH_2 has been aligned to the carbon core-levels of MIL-125. A Gaussian smearing of 0.05 eV has been used in the plot.

Table 1: Energy values in eV of the fundamental, E_g, and optical, E_{opt} band gap of MIL-125 and MIL-125-NH_2 at 0 K, E_g^0 and E_{opt}^0, and including thermal Δ^T and quantum nuclear Δ^{NQE} effects.

	MIL-125	MIL-125-NH_2
E_g^0	5.40	4.25
$E_g^0 + \Delta^T$	5.03	3.88
$E_g^0 + \Delta^T + \Delta^{NQE}$	4.65	3.50
E_{opt}^0	4.44	3.36
$E_{opt}^0 + \Delta^T + \Delta^{NQE}$	3.69	2.61
E_{opt}^{exp} [41]	ca. 3.6 eV	ca. 2.6 eV

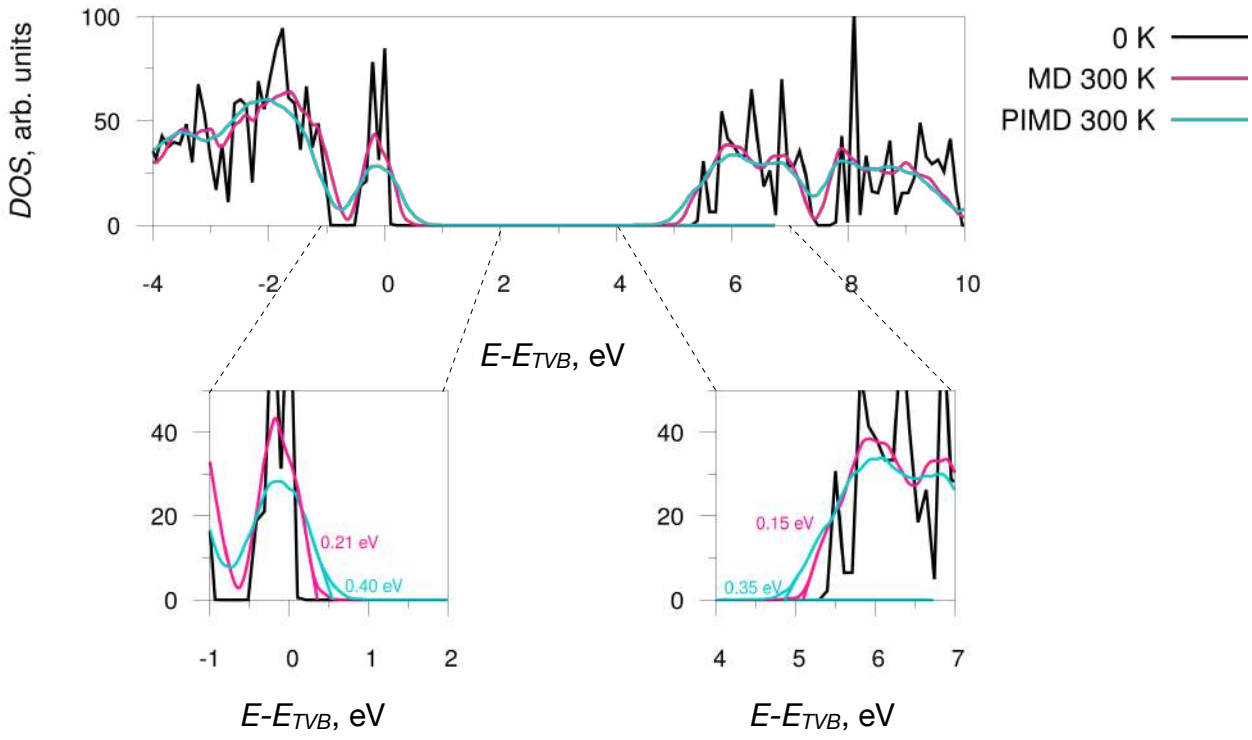

Figure 3: Total density of state of MIL-125 calculated at 0 K and at 300 K using classical nuclei molecular dynamics (MD) and path-integral molecular dynamics (PIMD). The two insets show a zoom-in into the proximity of the top of the valence band (Left) and of the bottom of the conduction band (Right).

Table 2: Relaxation energy of negative polaron (E^{-}_{rel}) , positive polaron (E^{+}_{rel}), and negative/positive polaron pair (E_{rel}) and interaction energy (E_{int}) of negative and positive polarons in MIL-125 and MIL-125-NH_2.

	MIL-125	MIL-125-NH_2	MIL-125-NH_2-[10%]$(OH)_2$
E^{-}_{rel}	-0.3445	-0.4985	-0.4464
E^{+}_{rel}	-0.0370	-0.1883	-0.1535
E^{T}_{rel}	-0.4172	-0.2246	-0.2815
E_{int}	$\mathbf{-0.0357}$	$\mathbf{+0.4622}$	$\mathbf{+0.3184}$

Interaction between charge carriers

We next focus on the nature of the charge carriers in MIL-125 and MIL-125-NH_2. After illumination, an electron is photoexcited into the CB leaving a hole into the VB. The two charges perturb the lattice, which undergoes a deformation in order to screen them. The resulting quasi-particles take the name of polarons. In addition, the negative (e^-) and the positive (h^+) polarons interact. We first study the polarons without interaction: we, separately, inject a hole and an electron in the MOFs and we relax the structure by using the same hybrid functional used in the electronic states calculation. We define the polaronic relaxation energy as the energy difference between the charged system ($\pm$) in its relaxed polaronic geometry (pol) and in the initial ground state geometry (gs):

$$E^{\pm}_{rel} = E^{\pm}_{pol} - E^{\pm}_{gs} \tag{2}$$

Table 2 reports the relaxation energies for the negative (E^-) and the positive (E^+) polarons for the two MOFs. The negative polaron relaxes of -0.34 eV and -0.50 eV for MIL-125 and MIL-125-NH_2, respectively. As shown in Fig. 4a and 4b, the electron induces a distortion that breaks the crystal symmetry. As a result, the charge localizes in a section of the metal cluster. To further describe the observed polaronic states, we also evaluate the corresponding binding energies, employing a grand-canonical formulation of defects in semiconductors (see the SI for details). The electron polaron is found 0.44 and 0.69 eV below the conduction band edge, in MIL and MIL-NH_2, respectively. Since the conduction band edge for these materials is made up of the same states at almost equivalent energy, also the electron polarons are found at very similar energies. For the hole, the relaxation energies are -0.04 eV and -0.19 eV for de-aminated and aminated MOFs, respectively. In both cases, the hole localizes into one of the linkers of the crystal, as shown in Fig 4a and 4b. The higher stabilization in MIL-125-NH_2 may be ascribed to the electron-donor nature of the amino group. Hole polarons are found to occur as shallow states with binding energies of

0.08 and 0.15 eV, for MIL and MIL-NH_2, respectively.

Subsequently, we study how the charge-carriers interact. To this purpose, we consider the system in the triplet state. In fact, the triplet state corresponds to the lowest energy electronic configuration for the photoexcited electron-hole couple.[24] As before, we calculate the relaxation energy by subtracting from the triplet state optimized geometry energy the ground state geometry energy in the same spin state, here called E^T_{rel}. We then calculate the interaction energy, defined as $E_{int} = E^T_{rel} - (E^+_{rel} + E^-_{rel})$. The results, in Table 2, clearly indicate an attractive interaction (-0.04 eV) between the charge-carrier in MIL-125; on the other hand, the interaction between photoelectron and photohole is repulsive in MIL-125-NH_2 ($+0.46$ eV). By observing the isodensity representation of the hole and electron wavefunction, Fig. 4c and 4d, we notice that in MIL-125 the two overlap significantly while in MIL-125-NH_2 they occupy two almost orthogonal regions of the crystal. In particular, the electron localizes onto the metal cluster and the hole on one of the linkers. A similar phenomenon has recently been observed in metal halide perovskites.[47] This result suggests that the charge-carrier interaction might be the key to determine the excited state lifetime in this class of materials.

Table 3: Oscillator strength (f), energy of the $S_0 \rightarrow S_1$ and $S_0 \rightarrow T_1$ transitions in eV, calculated at the optimized triplet geometry of MIL-125 and MIL-125-NH_2.

	MIL-125	MIL-125-NH_2
$f_{S_0 \rightarrow S_1}$	0.12	0.015
$E_{S_0 \rightarrow S_1}$	3.80	2.87
$E_{S_0 \rightarrow T_1}$	1.47	1.36

To validate the hypothesis that charge-carrier interactions determine the excited state lifetime, we estimate the ratio between the radiative time decay of MIL-125-NH_2 ($\tau_{\text{MIL-125-NH}_2}$) and MIL-125 ($\tau_{\text{MIL-125}}$). Recent transient absorption spectroscopy measurements[24] reveal that $\tau_{\text{MIL-125-NH}_2}$ is at least one order of magnitude larger than $\tau_{\text{MIL-125}}$. The radiative time decay τ is equal to the inverse of the decay rate, k, $\tau = 1/k$. From LR-TDDFT calculations

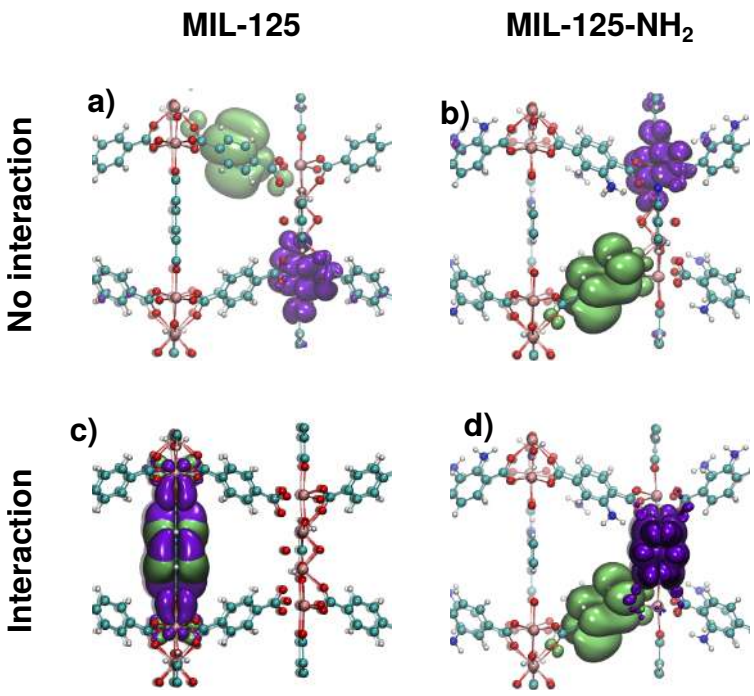

Figure 4: Isodensity representation of photoexcited electron (violet) and hole (green) in MIL-125 and MIL-125-NH_2. a) and b) Non interacting charge-carriers, calculated separately. c) and d) Interacting charge-carriers: triplet calculations (see main text).

we obtain the oscillator strength f of the radiative transition from the excited states to the ground state, which is proportional to the radiative rate, $f \propto k(\nu^2)^{-1}$, where ν is the wavenumber of the transition. It follows that we can write the ratio as

$$\frac{\tau_{\text{MIL-125-N}H_2}}{\tau_{\text{MIL-125}}} = \frac{k_{\text{MIL-125}}}{k_{\text{MIL-125-N}H_2}} = \frac{f_{\text{MIL-125}}}{f_{\text{MIL-125-N}H_2}} \frac{\nu^2_{\text{MIL-125-N}H_2}}{\nu^2_{\text{MIL-125}}} \tag{3}$$

Here we call the electronic ground state, which is in a singlet state, S_0; the first singlet excited state is S_1 and the lowest triplet state T_1. As previously described, the charge-carrier pair relaxes, after photoexcitation, into T_1. We calculate, using LR-TDDFT, the oscillator strengths of the optical transitions at the relaxed T_1 geometry. Since the oscillator strength is proportional to the square of the dipole moment, it is independent of the direction of the transition, meaning that $f_{T_1 \to S_0} = f_{S_0 \to T_1}$. Calculation of the oscillator strength for singlet to triplet states transitions is not possible without including spin-orbit coupling (SOC). However, SOC correction is very similar in the two MOFs (the ratio between them is then

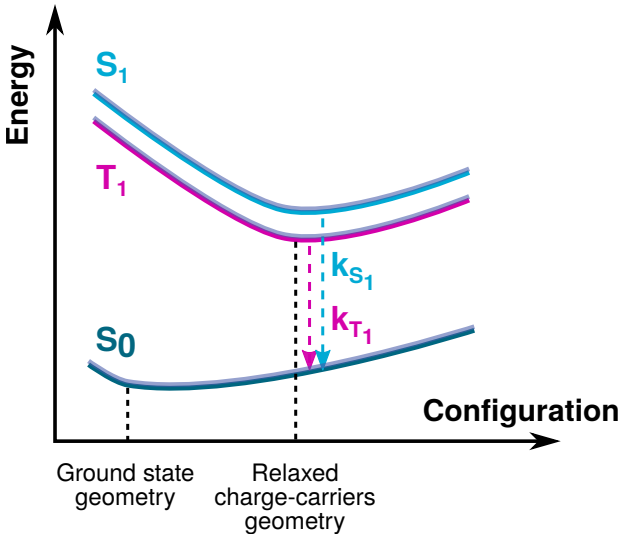

Figure 5: Scheme of the electronic states considered in the LR-TDDFT calculations for the estimation of the time decay ratio.

1). In addition, we check that the spatial component of the wavefunction of S_1 and T_1 for these MOFs is the same, and thus we can finally approximate f_{T_1} with f_{S_1}. A scheme of the possible optical transitions is shown in Fig. 5

We calculate f and transition energies for $S_0 \rightarrow S_1$ and $S_0 \rightarrow T_1$; values are reported in Table 3. By applying Eq. 3 we find that the time decay ratio is 14.02 for the $S_1 \rightarrow S_0$ transition and 8.72 for $T_1 \rightarrow S_0$. These ratios are in agreement with the transient absorption results.

Prediction

To test our charge-carriers separation model on an unknown MIL-125 MOF, we studied a modified version of MIL-125-NH_2 by substituting about 10% of bdc-NH_2 linker with bdc-$(OH)_2$. Hydroxy groups, as amino groups, are strong π activating substituents. This suggests that, like MIL-125-NH_2, also the corresponding bdc-$(OH)_2$ modified MOF might have photocatalytic properties. To this purpose, we calculate the charge-carrier relaxation and interaction energies (see Table 2). Indeed the charge-carrier interaction energy is positive,

0.32 eV, indicating a repulsion between the photoexcited charges. Both negative and positive polarons relaxation energies are very similar to the ones observed in MIL-125 and MIL-125-NH_2. However, like for MIL-125-NH_2, the charge-carrier pair relaxation energy E_{rel}^{T} is quite small. As a consequence, the interaction energy is positive. Comparing to MIL-125-NH_2, the repulsion energy is 0.15 eV smaller suggesting a shorter lifetime of the excited state.

It is interesting to note that we make this prediction for a material that has not yet been synthesized. To confirm these predictions, we synthesized MIL-125-NH_2-[10%]$(OH)_2$, and we perform transient absorption spectroscopy for this material (see the SI for details on the synthesis and the measurements), as well as its pure-amino counterpart MIL-125-NH_2. The measurements, reported in Fig. 6, show that indeed, the excited state of MIL-125-NH_2-[10%]$(OH)_2$ decays faster than MIL-125-NH_2, nicely confirming the predictions of our computational model. We fitted the decay curves with a double exponential function. The fast components, accounting for the first 1 μs, as shown in the inset of Fig. 6, are 523 $\pm$ 11 ns and 297 $\pm$ 15 ns for MIL-125-NH_2 and MIL-125-NH_2-[10%]$(OH)_2$, respectively.

Conclusion

In this work, we completely analyzed the electronic structure of two MOFs, MIL-125 and MIL-125-NH_2 before and after photoexcitation. Experimental measurements have shown that MIL-125-NH_2 can be used as antenna in photocatalytic systems. In such system the MOF captures the light and creates an electron and a hole, the electron is subsequently transported to a co-catalyst where, for example, a water splitting reaction takes place (see for example ref.[2] and references therein). If we use MIL-125, on the other hand, no catalytic activity is observed.[2,8,12,21,22] We first calculated the fundamental and optical energy gap, at 0 K and room temperature, employing an advanced theoretical framework based on a physical consideration. We found that the calculated optical gap is in striking agreement with the experimental one. Then, we analyzed the relaxation of the photogenerated electron/hole

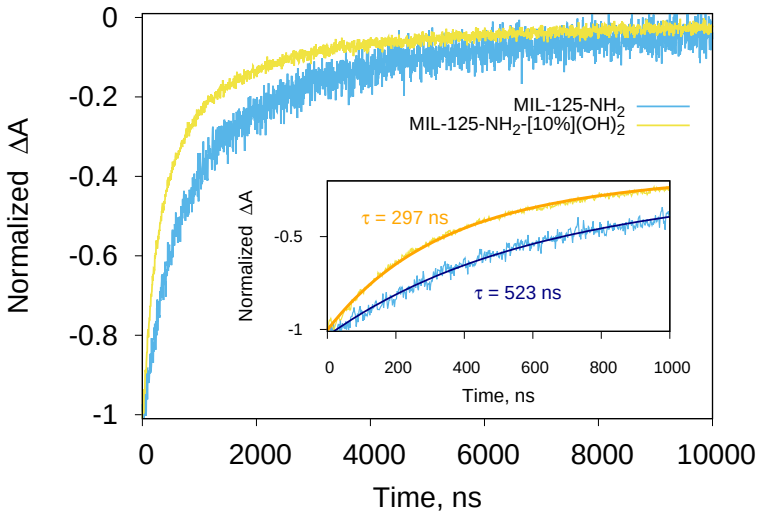

Figure 6: Transient absorption measurements of MIL-125-NH2 (blue) and MIL-125-NH_2-[10%]$(OH)_2$ (yellow), measured at 450 nm, following excitation at 420 nm. In the inset, a zoom of the first 1 μs is shown together with the fitting functions.

pair. We observed two opposite behaviour in MIL-125 and MIL-125-NH_2. While in the former, there is an attraction of the electron and hole pair, in MIL-125-NH_2 the interaction energy of the charge carriers is positive. The attraction/repulsion of the electron/hole pair has consequences for the radiative decay time. In fact, the radiative decay time depends on the recombination rate of the charge carriers. Charge carriers that attract each other tend to occupy the same spatial region in the crystal increasing the probability of recombination; vice-versa, distant charge carriers are less likely to recombine. Finally, by using LR-TDDFT, we have shown that indeed, the recombination rate in MIL-125-NH_2 is about one order of magnitude larger than in MIL-125 as previously observed in transient absorption measurements.[1] In addition, we correctly predict for MIL-125-NH_2-[10%]$(OH)_2$ a shorter lifetime than for MIL-125-NH_2.

Supporting Information Available

- details on the computational methods that have been used and further results
- details on the experimental procedures

Acknowledgement

The authors would like to thank Andres Ortega for verifying some of the calculations. This work has been performed in the context of the National Center of Competence in Research (NCCR): Materials' Revolution: Computational Design and Discovery of Novel Materials (MARVEL) of the Swiss National Science Foundation. We used computational resources of the Swiss National Supercomputing Center (CSCS) under grant number s879 and of SCITAS/EPFL. GC was supported by the Korean-Swiss Science and Technology Programme' (KSSTP) grant no. 162130 of the Swiss National Science Foundation (SNSF) SK and KCS thank Swiss National Science Foundation (SNF) for funding under the Ambizione Energy Grant n.PZENP2_166888 and Materials' Revolution: Computational Design and Discovery of Novel Materials (MARVEL).

References

(1) Santaclara, J. G.; Nasalevich, M. A.; Castellanos, S.; Evers, W. H.; Spoor, F. C. M.; Rock, K.; Siebbeles, L. D. A.; Kapteijn, F.; Grozema, F.; Houtepen, A. et al. Organic Linker Defines the Excited-State Decay of Photocatalytic MIL-125(Ti)-Type Materials. *ChemSusChem* **2016**, *9*, 388–395.

(2) Kampouri, S.; Nguyen, T. N.; Ireland, C. P.; Valizadeh, B.; Ebrahim, F. M.; Capano, G.; Ongari, D.; Mace, A.; Guijarro, N.; Sivula, K. et al. Photocatalytic hydrogen generation

from a visible-light responsive metal-organic framework system: the impact of nickel phosphide nanoparticles. *J. Mater. Chem. A* **2018**, *6*, 2476–2481.

(3) Bolton, J. R. Solar photoproduction of hydrogen: A review. *Sol. Energy* **1996**, *57*, 37–50.

(4) Ni, M.; Leung, M. K. H.; Leung, D. Y. C.; Sumathy, K. A review and recent developments in photocatalytic water-splitting using TiO2 for hydrogen production. *Renew. Sust. Energ. Rev.* **2007**, *11*, 401–425.

(5) Andreiadis, E. S.; Chavarot-Kerlidou, M.; Fontecave, M.; Artero, V. Artificial Photosynthesis: From Molecular Catalysts for Light-driven Water Splitting to Photoelectrochemical Cells. *Photochem. Photobiol.* **2011**, *87*, 946–964.

(6) Kondarides, D. I.; Daskalaki, V. M.; Patsoura, A.; Verykios, X. E. Hydrogen Production by Photo-Induced Reforming of Biomass Components and Derivatives at Ambient Conditions. *Catal. Lett.* **2008**, *122*, 26–32.

(7) Stern, L.-A.; Feng, L.; Song, F.; Hu, X. Ni 2 P as a Janus catalyst for water splitting: the oxygen evolution activity of Ni 2 P nanoparticles. *Energy Environ. Sci.* **2015**, *8*, 2347–2351.

(8) Meyer, K.; Bashir, S.; Llorca, J.; Idriss, H.; Ranocchiari, M.; van Bokhoven, J. A. Photocatalyzed Hydrogen Evolution from Water by a Composite Catalyst of NH2-MIL-125(Ti) and Surface Nickel(II) Species. *Chem.: Eur. J.* **2016**, *22*, 13894–13899.

(9) Kampouri, S.; Nguyen, T. N.; Spodaryk, M.; Palgrave, R. G.; Züttel, A.; Smit, B.; Stylianou, K. C. Concurrent Photocatalytic Hydrogen Generation and Dye Degradation Using MIL-125-NH2 under Visible Light Irradiation. *Adv. Funct. Mater.* **2018**, *28*, 1806368.

(10) Kampouri, S.; Stylianou, K. C. Dual-Functional Photocatalysis for Simultaneous Hydrogen Production and Oxidation of Organic Substances. *ACS Catal.* **2019**, *9*, 4247–4270.

(11) McDonald, T. M.; Lee, W. R.; Mason, J. A.; Wiers, B. M.; Hong, C. S.; Long, J. R. Capture of Carbon Dioxide from Air and Flue Gas in the Alkylamine-Appended Metal–Organic Framework mmen-Mg2(dobpdc). *J. Am. Chem. Soc.* **2012**, *134*, 7056–7065.

(12) Kim, S.-N.; Kim, J.; Kim, H.-Y.; Cho, H.-Y.; Ahn, W.-S. Adsorption/catalytic properties of MIL-125 and NH2-MIL-125. *Catal. Today* **2013**, *204*, 85–93.

(13) Fu, Y.; Sun, D.; Chen, Y.; Huang, R.; Ding, Z.; Fu, X.; Li, Z. An Amine-Functionalized Titanium Metal–Organic Framework Photocatalyst with Visible-Light-Induced Activity for CO2 Reduction. *Angew. Chem.* **2012**, *124*, 3420–3423.

(14) Alvaro, M.; Carbonell, E.; Ferrer, B.; Llabrés i Xamena, F. X.; Garcia, H. Semiconductor behavior of a metal-organic framework (MOF). *Chem.: Eur. J.* **2007**, *13*, 5106–5112.

(15) Gomes Silva, C.; Corma, A.; Garcia, H. Metal organic frameworks as semiconductors. *J. Mater. Chem.* **2010**, *20*, 3141–3156.

(16) Aubrey, M. L.; Long, J. R. A Dual Ion Battery Cathode via Oxidative Insertion of Anions in a Metal Organic Framework. *J. Am. Chem. Soc.* **2015**, *137*, 13594–13602.

(17) Dhakshinamoorthy, A.; Asiri, A. M.; García, H. Metal–Organic Framework (MOF) Compounds: Photocatalysts for Redox Reactions and Solar Fuel Production. *Angew. Chem. Int. Ed.* **2016**, *55*, 5414–5445.

(18) Horiuchi, Y.; Toyao, T.; Saito, M.; Mochizuki, K.; Iwata, M.; Higashimura, H.; Anpo, M.; Matsuoka, M. Visible-Light-Promoted Photocatalytic Hydrogen Production

by Using an Amino-Functionalized Ti(IV) Metal–Organic Framework. *J. Phys. Chem. C* **2012**, *116*, 20848–20853.

(19) Dan-Hardi, M.; Serre, C.; Frot, T.; Rozes, L.; Maurin, G.; Sanchez, C.; Férey, G. A New Photoactive Crystalline Highly Porous Titanium(IV) Dicarboxylate. *J. Am. Chem. Soc.* **2009**, *131*, 10857–10859.

(20) Zlotea, C.; Phanon, D.; Mazaj, M.; Heurtaux, D.; Guillerm, V.; Serre, C.; Horcajada, P.; Devic, T.; Magnier, E.; Cuevas, F. et al. Effect of NH 2 and CF 3 functionalization on the hydrogen sorption properties of MOFs. *Dalton Trans.* **2011**, *40*, 4879–4881.

(21) Nasalevich, M. A.; Becker, R.; Ramos-Fernandez, E. V.; Castellanos, S.; Veber, S. L.; Fedin, M. V.; Kapteijn, F.; Reek, J. N. H.; Vlugt, J. I. v. d.; Gascon, J. Co@NH2-MIL-125(Ti): cobaloxime-derived metal–organic framework-based composite for light-driven H2 production. *Energy Environ. Sci.* **2014**, *8*, 364–375.

(22) Fu, Y.; Sun, L.; Yang, H.; Xu, L.; Zhang, F.; Zhu, W. Visible-light-induced aerobic photocatalytic oxidation of aromatic alcohols to aldehydes over Ni-doped NH2-MIL-125(Ti). *Appl. Catal. B-Environ.* **2016**, *187*, 212–217.

(23) de Miguel, M.; Ragon, F.; Devic, T.; Serre, C.; Horcajada, P.; Garcia, H. Evidence of Photoinduced Charge Separation in the Metal–Organic Framework MIL-125(Ti)-NH2. *ChemPhysChem* **2012**, *13*, 3651–3654.

(24) Nasalevich, M. A.; Hendon, C. H.; Santaclara, J. G.; Svane, K.; Linden, B. v. d.; Veber, S. L.; Fedin, M. V.; Houtepen, A. J.; Veen, M. A. v. d.; Kapteijn, F. et al. Electronic origins of photocatalytic activity in d^0 metal organic frameworks. *Sci. Rep.* **2016**, *6*, 23676.

(25) Castells-Gil, J.; Padial, N. M.; Almora-Barrios, N.; Albero, J.; Ruiz-Salvador, A. R.; Gonzalez-Platas, J.; Garcia, H.; Marti-Gastaldo, C. Chemical Engineering of Photoac-

tivity in Heterometallic Titanium-Organic Frameworks by Metal Doping. *Angew Chem Int Edit* **2018**, *57*, 8453–8457.

(26) Choi, J. H.; Choi, Y. J.; Lee, J. W.; Shin, W. H.; Kang, J. K. Tunability of Electronic Band Gaps from Semiconducting to Metallic States via Tailoring Zn Ions in MOFs with Co Ions. *Phys Chem Chem Phys* **2009**, *11*, 628–631.

(27) Fuentes-Cabrera, M.; Nicholson, D. M.; Sumpter, B. G.; Widom, M. Electronic Structure and Properties of Isoreticular Metal-Organic Frameworks: The case of M-IRMOF1 (M=Zn, Cd, Be, Mg, and Ca). *J Chem Phys* **2005**, *123*.

(28) Hendon, C. H.; Tiana, D.; Vaid, T. P.; Walsh, A. Thermodynamic and electronic properties of tunable II-VI and IV-VI semiconductor based metal-organic frameworks from computational chemistry. *J Mater Chem C* **2013**, *1*, 95–100.

(29) Yang, L. M.; Ravindran, P.; Vajeeston, P.; Tilset, M. Ab initio investigations on the crystal structure, formation enthalpy, electronic structure, chemical bonding, and optical properties of experimentally synthesized isoreticular metal-organic framework-10 and its analogues: M-IRMOF-10 (M = Zn, Cd, Be, Mg, Ca, Sr and Ba). *Rsc Adv* **2012**, *2*, 1618–1631.

(30) Grau-Crespo, R.; Aziz, A.; Collins, A. W.; Crespo-Otero, R.; Hernandez, N. C.; Rodriguez-Albelo, L. M.; Ruiz-Salvador, A. R.; Calero, S.; Hamad, S. Modelling a Linker Mix-and-Match Approach for Controlling the Optical Excitation Gaps and Band Alignment of Zeolitic Imidazolate Frameworks. *Angew Chem Int Edit* **2016**, *55*, 16012–16016.

(31) Kuc, A.; Enyashin, A.; Seifert, G. Metal-organic frameworks: Structural, energetic, electronic, and mechanical properties. *J Phys Chem B* **2007**, *111*, 8179–8186.

(32) Li, Y.; Fu, Y. Q.; Ni, B. L.; Ding, K. N.; Chen, W. K.; Wu, K. C.; Huang, X.;

Zhang, Y. F. Effects of ligand functionalization on the photocatalytic properties of titanium-based MOF: A density functional theory study. *Aip Adv* **2018**, *8*.

(33) Ryder, M. R.; Dona, L.; Vitillo, J. G.; Civalleri, B. Understanding and Controlling the Dielectric Response of Metal-Organic Frameworks. *Chempluschem* **2018**, *83*, 308–316.

(34) Vanpoucke, D. E. P. Linker Functionalization in MIL-47(V)-R Metal-Organic Frameworks: Understanding the Electronic Structure. *J Phys Chem C* **2017**, *121*, 8014–8022.

(35) Zhang, T. X.; Jin, Y. H.; Shi, Y. S.; Li, M. C.; Li, J. N.; Duan, C. Y. Modulating photoelectronic performance of metal-organic frameworks for premium photocatalysis. *Coordin Chem Rev* **2019**, *380*, 201–229.

(36) Guo, Z. D.; Ambrosio, F.; Chen, W.; Gono, P.; Pasquarello, A. Alignment of Redox Levels at Semiconductor-Water Interfaces. *Chem Mater* **2018**, *30*, 94–111.

(37) Wiktor, J.; Reshetnyak, I.; Ambrosio, F.; Pasquarello, A. Comprehensive modeling of the band gap and absorption spectrum of BiVO4. *Phys Rev Mater* **2017**, *1*.

(38) Perdew, J. P.; Zunger, A. Self-Interaction Correction to Density-Functional Approximations for Many-Electron Systems. *Phys Rev B* **1981**, *23*, 5048–5079.

(39) Zhang, Y. K.; Yang, W. T. A challenge for density functionals: Self-interaction error increases for systems with a noninteger number of electrons. *J Chem Phys* **1998**, *109*, 2604–2608.

(40) Ambrosio, F.; Meggiolaro, D.; Mosconi, E.; De Angelis, F. Charge Localization, Stabilization, and Hopping in Lead Halide Perovskites: Competition between Polaron Stabilization and Cation Disorder. *Acs Energy Lett* **2019**, *4*, 2013–2020.

(41) Hendon, C. H.; Tiana, D.; Fontecave, M.; Sanchez, C.; D'arras, L.; Sassoye, C.; Rozes, L.; Mellot-Draznieks, C.; Walsh, A. Engineering the Optical Response of the

Titanium-MIL-125 Metal–Organic Framework through Ligand Functionalization. *J. Am. Chem. Soc.* **2013**, *135*, 10942–10945.

(42) Miceli, G.; Chen, W.; Reshetnyak, I.; Pasquarello, A. Nonempirical hybrid functionals for band gaps and polaronic distortions in solids. *Phys. Rev. B* **2018**, *97*, 121112.

(43) Perdew, J. P.; Ernzerhof, M.; Burke, K. Rationale for mixing exact exchange with density functional approximations. *J. Chem. Phys.* **1996**, *105*, 9982–9985.

(44) Aziz, A.; Ruiz-Salvador, A. R.; Hernández, N. C.; Calero, S.; Hamad, S.; Grau-Crespo, R. Porphyrin-based metal-organic frameworks for solar fuel synthesis photocatalysis: band gap tuning via iron substitutions. *J. Mater. Chem. A* **2017**, *5*, 11894–11904.

(45) Gu, Z.-G.; Heinke, L.; Wöll, C.; Neumann, T.; Wenzel, W.; Li, Q.; Fink, K.; Gordan, O. D.; Zahn, D. R. Experimental and theoretical investigations of the electronic band structure of metal-organic frameworks of HKUST-1 type. *Appl. Phys. Lett.* **2015**, *107*, 102_1.

(46) Dolgopolova, E. A.; Brandt, A. J.; Ejegbavwo, O. A.; Duke, A. S.; Maddumapatabandi, T. D.; Galhenage, R. P.; Larson, B. W.; Reid, O. G.; Ammal, S. C.; Heyden, A. et al. Electronic Properties of Bimetallic Metal–Organic Frameworks (MOFs): Tailoring the Density of Electronic States through MOF Modularity. *J. Am. Chem. Soc.* **2017**, *139*, 5201–5209, PMID: 28316244.

(47) Ambrosio, F.; Wiktor, J.; Angelis, F. D.; Pasquarello, A. Origin of low electron–hole recombination rate in metal halide perovskites. *Energy Environ. Sci.* **2018**, *11*, 101–105.

(48) Ambrosio, F.; Miceli, G.; Pasquarello, A. Structural, Dynamical, and Electronic Properties of Liquid Water: A Hybrid Functional Study. *J. Phys. Chem. B* **2016**, *120*, 7456–7470.

(49) Wiktor, J.; Rothlisberger, U.; Pasquarello, A. Predictive determination of band Gaps of inorganic halide perovskites. *J. Phys. Chem. Lett.* **2017**, *8*, 5507–5512.

(50) Iannuzzi, M.; Chassaing, T.; Wallman, T.; Hutter, J. Ground and excited state density functional calculations with the Gaussian and augmented-plane-wave method. *CHIMIA* **2005**, *59*, 499–503.